THROUGH-THE-WALL SAR ATTRIBUTED SCATTERING CENTER FEATURE ESTIMATION

Emre Ertin and Randolph L. Moses

The Ohio State University
Department of Electrical and Computer Engineering

ABSTRACT

We consider characterization of building interior structure from two-pass interferometric circular SAR data. We extract dihedral and trihedral scattering primitives that dominate monostatic returns from buildings. The 3D location of each scattering primitive is estimated using the phase information in two-pass data. Using simplified wall and primitive models, we match model signatures to the extracted features using a hypothesis selection and refinement loop. Examples illustrate the effectiveness of the feature extraction approach.

Index Terms— Circular SAR, Through-the-wall Imaging, Feature Estimation, Wide-angle Imaging

1. INTRODUCTION

We consider the feasibility of determining the interior structure of a building using radar measurements. Radar measurements have the advantage of all weather and day/night visibility. Furthermore, for sufficiently low center frequencies, radar systems have been successfully employed for mapping and object detection through foliage. Radar imaging through building walls and ceilings, however, is a challenging problem due to the anisotropic and periodic scattering response of many types of walls, the significant attenuation loss of building walls and ceilings, and the high clutter and multipath effects of complex building and interior structure.

In this paper we consider for building structure estimation from an airborne synthetic aperture radar (SAR) system. At the standoff distances and limited interrogation angles available for airborne SAR, high-fidelity reconstructions of building interior structure is ill-conditioned; instead, we adopt the approach of estimating dominant scattering features (trihedrals and dihedrals) that can be used to infer building interior structure. Trihedral features describe dominant scattering from corners in the building (such as wall-wall-floor corners), whereas dihedrals capture the dominant response from wall-floor structures. The feature extraction approach affords robustness to clutter and multipath, and takes advantage of prior knowledge of physical scattering models to improve the conditioning of this ill-posed deconvolution problem.

While the proposed feature extraction approach applies for general airborne SAR apertures, we consider the special case of two-pass, monostatic, circular apertures. A two-pass measurement is realized by an airborne radar flying a circular path above an urban area containing buildings. Measurements at two closely-spaced elevation angles enables interferometric SAR (IFSAR) processing techniques, providing for computationally tractable processing approaches and providing valuable 3D feature localization without the need for expensive 3D SAR collection geometries.

We propose a statistical signal processing algorithm for estimating the interior features from interferometric, circular SAR measurements. We divide the circular aperture into subapertures and estimate the locations and structure of scattering primitives from monostatic radar returns. Height filtering and height-dependent deconvolution of assumed building propagation are used to refine the subaperture SAR images; this results in improved feature detection and localization. The result is a list of scattering primitives indexed by look angle and position. Using a simplified wall model we evaluate the likelihood of each hypothesized interior model by matching the model signatures to the extracted features.

2. CIRCULAR SAR SYSTEM MODEL

We consider a SAR system which collects coherent backscatter measurements $g_{i,j}(f_k)$ on circular apertures parameterized with azimuth angles $\{\phi_i\}$ covering $[0, 2\pi]$ and at two elevation angles $\theta_j = \{\theta_c - \Delta\theta/2, \theta_c + \Delta\theta/2\}$, $j = 1, 2$. The backscatter measurements are at discrete set of frequencies $\{f_k\}$. The set of radar returns $\{g_{i,j}(f_k)\}$ correspond to projections of the underlying three dimensional reflectivity function of the spotlighted scene $f(x, y, z)$. Specifically, each pass of the backscatter measurements provide samples of $F(k_x, k_y, k_z)$ [1], the 3-D spatial Fourier transform of the reflectivity function on a two-dimensional conical manifold at points $k_x = \frac{4\pi f_k}{c}\cos(\phi_i)\cos(\theta_j)$, $k_y = \frac{4\pi f_k}{c}\sin(\phi_i)\cos(\theta_j)$, $k_z = \frac{4\pi f_k}{c}\sin(\theta_j)$. Since each circular SAR data set lies on a 2D manifold, 2D ground plane images $I_1(x, y)$ and $I_2(x, y)$ constructed from the inverse Fourier transform of the projection of each conical manifold to (k_x, k_y) plane will preserve the entire information from the backscatter measurements.

$$I_j(x,y) = \mathcal{F}^{-1}_{(x,y)}\left[F_j(k_x, k_y, \sqrt{k_x^2+k_y^2}\tan(\theta_j))\right] \quad (1)$$

However, the wide-angle coherent image $I_j(x,y)$ is not an efficient data representation for the radar returns, because it requires a high spatial sampling rate (on the order of $c/(4f_c)$ where f_c is the center frequency of the radar) to prevent aliasing of the circular bandpass signature. Furthermore, wide-angle coherent imaging is matched to an isotropic point reflector assumption, whereas most scattering is anisotropic [2]. We instead propose to represent the SAR measurements at each elevation angle by the image sequence set $\{I_{j,m}(x,y)\}$ where each image is the output of a filter matched to a limited-persistence reflector over the azimuth angles in window $\mathcal{W}_m(\theta)$. Specifically, the m-th subaperture image is constructed using

$$I_{j,m}(x,y) = \mathcal{F}^{-1}_{(x,y)}\left[F_j(k_x,k_y)\mathcal{W}_m(\tan^{-1}(k_x/k_y))\right] \quad (2)$$

where the azimuthal window function $\mathcal{W}_m(\phi)$ is defined as:

$$\mathcal{W}_m(\phi) = \begin{cases} W\left(\frac{\phi-\phi_m}{\Delta}\right), & -\Delta/2 < \phi < \Delta/2 \\ 0, & \text{otherwise} \end{cases} \quad (3)$$

with ϕ_m being the center azimuth angle for the m-th window and Δ being the hypothesized persistence width. The window function $W(\cdot)$ is an invertible tapered window used for cross-range sidelobe reduction. Note that, unlike the full 360°, each subimage in (2) can be modulated to baseband and sampled at a much coarser spatial sampling than $c/(4f_c)$, and instead determined by the SAR downrange and crossrange resolutions. Each baseband image $I^B_{i,m}(x,y)$ is calculated as:

$$I^B_{j,m}(x,y) = I_{j,m}(x,y)e^{-j(k_x^0 x + k_y^0 y)}. \quad (4)$$

where the center frequency (k_x^0, k_y^0) is determined by the center aperture ϕ_m, mean elevation angle θ_c and center frequency f_c as $k_x^0 = \frac{4\pi f_c}{c}\cos(\theta_c)\cos(\phi_m)$, $k_y^0 = \frac{4\pi f_c}{c}\cos(\theta_c)\sin(\phi_m)$. We use the set of baseband modulated subaperture ground plane images $\{I^B_{j,m}(x,y)\}$ to extract building features as described in the next section.

3. THROUGH-THE-WALL FEATURE EXTRACTION

The subaperture images form the inputs to a procedure for feature extraction of trihedral and dihedral scattering features from building substructures. The processing steps are summarized in Figure 1. We assume that nominal information about the number of floors and their associated heights is available. Each pair of subaperture images is filtered, to identify features from different heights, using a spatially-varying difference of the relative phase between the two images. Then the images are deconvolved using a point spread function selected to match the propagation effects expected for scattering features at that height. After deconvolution, high energy regions are selected for feature detection and divided into Dihedral and Trihedral features based on their scattering responses as a function of supaperture center azimuth. These initial detections are refined using parameteric non-linear regression to estimate feature locations, orientations, and (for dihedrals) length. These estimates are used to refine a building floor model which in turn can be used to refine the point spread functions used in the deconvolution process. Each of these steps is described in more detail below.

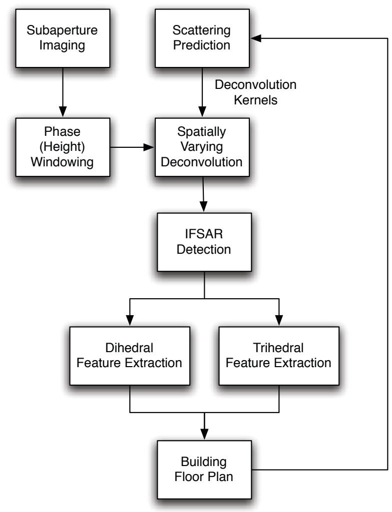

Fig. 1. Processing steps for extracting building features .

3.1. Phase-height windowing

Because the subaperture images $I^B_{1,m}(x,y)$, $I^B_{2,m}(x,y)$ are obtained from closely-spaced elevation angles, their magnitudes are similar, and the phase difference between image pixels encode height of scattering responses. For isolated scattering at a height z, this phase difference is related to z by

$$z = \frac{\lambda\cos(\theta_c)}{4\pi\Delta\theta}[\angle I^B_{1,m} - \angle I^B_{2,m}] \quad (5)$$

where λ is the wavelength of the radar center frequency and $I^B_{j.m}$ is the complex baseband image pixel value. We then filter the subaperture images using a window function on the relative phase, centered at the hypothesized height z_0 of interest, to isolate image responses around this height:

$$I^{B,z_0}_{i,m}(x,y) = I^B_{i,m}(x,y)\mathcal{W}\left(\angle I^B_{1,m} - \angle I^B_{2,m}, \frac{4\pi z_0\Delta\theta}{\lambda\cos(\theta_c)}\right) \quad (6)$$

where $\mathcal{W}$ is a height window function. This subaperture-based approach has the advantage of only a modest requirement on radar phase coherence; accurate radar phase coherence is needed only over azimuth extents corresponding to the subapertures, and not across the entire 360° circular aperture.

3.2. Deconvolution of Propagation Effects

The backscattered responses often result from dielectric corners formed from floors and walls which are in turn distorted and delayed by transmission through such dielectric media as other walls and ceilings; as a result, the scattering from even localized structures are dispersed in both range and crossrange. (see Figure 2(a)). In addition, scattering locations appear farther downrange in the image than the corresponding structure location due to the phase delays associated with transmission through dielectric media and to backscattering from dielectric materials. To mitigate these effects, we deconvolve each image using an convolution kernel determined from an initial hypothesis of wall and ceiling dielectric compositions; this kernel is different for different heights of interest. We use a sparse deconvolution method [3], which finds the solution to the minimization problem

$$\arg\min_{x} \left\{ \|I^z - Hx\|_2^2 + \mu \|x\|_p^p \right\} \tag{7}$$

where I^z is a vector of height-filtered image pixels, x is the vector of deconvolved image pixels, and H contains the assumed convolution kernel. The second term in the minimization favors sparse solutions for $p \leq 1$. An initial convolution operator H is obtained from a prior estimate of the outside wall/ceiling structure of the building, or from an isolated scattering response from the original SAR image. Figure 2(b) shows an example of this deconvolution to focus 2nd-floor scattering primitives. The assumed operator H emulates the distortion from a single rebar-reinforced concrete wall oriented at a 45° angle from the radar. In this case the assumed wall propagation properties were 20% mismatched from the actual wall properties. In spite of the mismatch, significant energy concentration is realized, allowing for improved detection and subsequent localization of scattering primitives.

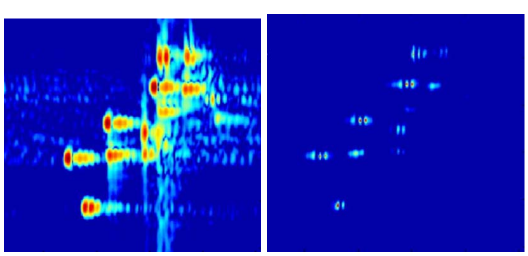

(a) (b)

Fig. 2. Example subaperture SAR image of a building model at center azimuth of 45° and elevation $45°$. (a) Original image; (b) Image after deconvolution using a nominal rebar convolution operator not matched to the building. Downrange increases from left to right.

3.3. Scattering Primitive Detection and Refinement

From the (x, y) position and height, along with the subaperture center azimuth ϕ_m of the image, 3D location estimates of large-amplitude image regions are obtained. Trihedrals are detected as regions with compact crossrange support and significant backscatter energy at off-cardinal look angles, while dihedrals appear in aspects limited to a single (usually cardinal angle) supaperture image. Location estimates are obtained for each subaperture, transformed a common 3D reference frame, and combined noncoherently across subapertures, to obtain an initial estimate of scattering locations of building structures in 3D. The result is a list of hypothesized scattering primitives indexed by azimuth angle and position.

The initial scattering features exhibit parameter bias that results from frequency distortions due to dielectric properties that make up the faces of the dihedral and trihedral scattering primitives. To correct this bias, we use a simplified wall model to predict a set of hypothesized feature responses. An augmented version of the Numerical Electromagnetic Code-Basic Scattering Code (NEC-BSC) [4] is used for the electromagnetic simulations of the radar scattering from hypothesized media transmission models as well as in constructing scattering primitive models; the code is augmented to include anisotropic dielectric materials and periodic structures such as rebar-reinforced walls. The NEC-BSC code is well suited for this feature-based approach because it computes specific scattering interactions within the framework of the uniform theory of diffraction in a highly computationally efficient manner ($<$ 1 sec per prediction). We evaluate the likelihood of each hypothesized interior model by matching the NEC-BSC model signatures to the extracted features. We then estimate and refine the transmission and reflection parameters of the hypothesized walls and primitive faces to minimize the squared error between the image and the image obtained from the NEC-BSC simulation, using a nonlinear iterative minimization approach. Reasoning over subapertures provides a means for discriminating between trihedral and dihedral features. We cluster responses by location, and identify primitives which persist over several subapertures, noting that trihedral structures persist over nearly 90°.

4. BUILDING EXAMPLE

We present results of interior corner estimation using synthetic radar backscattering predictions of a two-story building with dimensions 22.2 × 9.6 × 6.0 meters. Two monostatic, single polarization, circular SAR measurement apertures are synthesized using the augmented NEC-BSC code, at elevation angles $45.0°$ and $45.2°$. The outside walls and the first and second floor ceilings in the building are modeled as rebar-reinforced concrete, and interior walls are modeled as cinderblock walls. Noise was added to simulate a background clutter with RCS that is 40 dB below the peak amplitude of

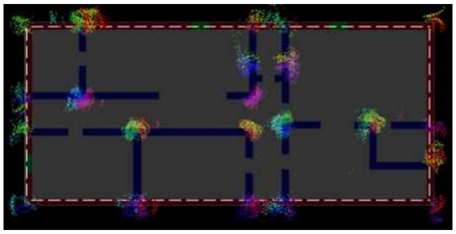

Second Floor

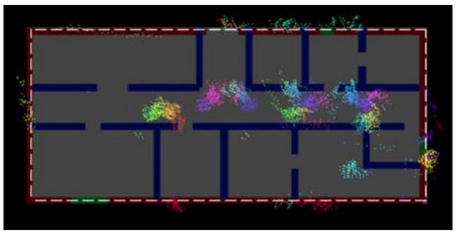

First Floor

Fig. 3. Initial trihedral primitive location estimates of the Handshake building. Color denotes SAR center azimuth at which the feature was detected.

the largest scattering return. Feature extraction and hypothesis refinement is implemented using 20° subaperture images formed at 10° increments. We present trihedral feature extraction and localization results; for trihedrals, we do not use the images centered at the four cardinal angles of the building.

Figure 3 shows the initial scattering location estimates for first-floor and second-floor trihedral corner freatures, before the deconvolution or hypothesis refinement steps. The initial estimates are 3D location estimates that are noncoherently combined; the figures shown are for height filtering centered at $z_0 = 3$ m and $z_0 = 0$, corresponding to the heights the second floor and first floor wall-floor junctions. Overlaid is the corresponding floor plan. Color encodes the subaperture's center azimuth angle from which a given scattering primitive is estimated. One sees that the trihedral features are detected for all second floor corners and many first floor corners. Noticeable location bias due to propagation delays are seen; this bias is more prominent for the first floor features, due to the additional propagation delays from transmission through two or more additional walls or ceilings.

After hypothesis refinement and 3D reasoning, one obtains a much sparser set of trihedral scattering primitive features, as shown in Figure 4 for the second floor. The trihedrals are denoted as one of four primitive icons (denoting trihedral orientation), and each icon corner is positioned at the final (x, y, z) location estimate of the primitive (only the (x, y) locations can be seen from this top view). The z estimates are all within 25 cm of the true heights for these primitives. Features are well-aligned with building corners, and no false-alarm trihedral detections are seen at locations that do not have floor-wall-wall corners. In addition, the location estimates show significant consistency for the differently-colored icons, which use independent data sets in forming the estimates; primitive estimates from, say, northeast pointing trihedrals are obtained using disjoint data for northwest or southeast corners, yet align well with each other in location. The primitive estimates shown in Figure 4 are obtained through automated processing, with no prior information about outside building dimensions or location.

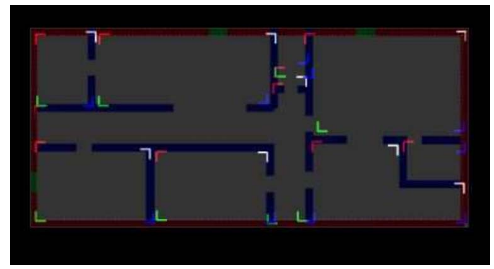

Fig. 4. Deconvolved SAR building image using a nominal rebar wall convolution operator.

5. CONCLUSION

We have presented an approach for estimating features key to inferring internal building floor plans from a standoff airborne, monostatic SAR system. Interferometric processing of two circular SAR apertures is used to infer 3D location information from sparse elevation measurements. Subaperture processing of the 360° SAR apertures was used to address anisotropic scattering responses and to permit bias reduction and hypothesis refinement by reasoning over subapertures. The approach was applied to the estimation of trihedrals to infer wall-wall-floor corners in a two-story building.

6. REFERENCES

[1] C. V. Jakowatz and P. A. Thompson, "A new look at spotlight mode synthetic aperture radar as tomography: imaging 3D targets," *IEEE Trans. Image Processing*, vol. 4, no. 5, May 1995.

[2] D. E. Dudgeon, R. T. Lacoss, C. H. Lazott, and J. G. Verly, "Use of persistant scatterers for model-based recognition," in *Proc. SPIE 2230*, April 1994, pp. 356–368.

[3] M. Cetin and W. C. Karl, "Feature enhanced synthetic aperture radar image formation based on nonquadratic regularization," *IEEE Trans. Image Processing*, vol. 10, pp. 623–631, Apr 2001.

[4] R. J. Marhefka, "Numerical Electromagnetic Code - Basic Scattering Code, (NEC-BSC version 4.2), users - manual," Technical Report, The Ohio State University ElectroScience Laboratory, June 2000.